

Generalized Box-Plot for Analysis of Unsteady CFD Solutions

S.T. Imlay^{*}, D.K. Rittenberg^{*}, C.A. Mackey^{*} and C.C. Nelson^{**}

^{*} Tecplot Inc., USA

^{**} Innovative Technology Applications Company, USA

Abstract: The functional box plot is generalized to provide a holistic view of the four dimensional space-time field data resulting from unsteady Computational Fluid Dynamics simulations. It displays the variation of five common statistics - minimum, first-quartile, median, third-quartile, and maximum – projected onto the three-dimensional spatial sub-space. Visual analysis using the generalized box plot is demonstrated for the unsteady flows past a swept cylinder and a wind turbine.

Keywords: Visualization, Box-Plot, Unsteady Flow, Computational Fluid Dynamics, Vortical Flows.

1 Introduction

The application of computational fluid dynamics (CFD) in the design process has increased dramatically over the last decade. This is due, in large part, to the relentless and continuing growth of computer performance. In some cases the enhanced computer power is used to perform high-resolution CFD calculations to analyze the details of complicated unsteady flow fields around complex configurations. In other cases it is used to create a virtual wind-tunnel where hundreds or thousands of lower resolution CFD computations are performed to estimate the aerodynamic properties of a prospective configuration throughout its operating envelope. The design-space defining the operating envelope is highly dimensional – it has many factors, or parameters, that define the operating conditions and configurations used for each run. The primary product of these parametric studies is not the details of the flow-field but a performance database of CFD meta-data, like force and moment coefficients. With this database, an engineer may analyze the performance and fluid-dynamic characteristics of the machine, or evaluate control system designs. However, to discover the root cause of anomalies in the meta-data and to better design fixes for undesirable flow behavior, the detailed flow-field must still be analyzed in many cases. This paper presents a new technique, the generalized box-plot, for dimensional reduction to provide a more holistic visual analysis of unsteady flow-field data in the highly-dimensional design space.

The components of the design space vary with the goal of the parametric analysis. For an aircraft, it will typically include the five standard flight parameters: α , β , M , Re , and Pr (or T). It will also generally include some configuration parameters, but the nature of these will vary with the goal of the parametric study. For example, if the analysis is focused on flight dynamics, stability and control, or G&C, the configuration parameters might be control-surface deflection angles. In this case the aerodynamic database may eventually be combined with a six degree-of-freedom analysis to evaluate the flight characteristics and/or G&C system for the vehicle or design. If the analysis is focusing on

high-lift configurations, it may include flap angles or landing gear position. Alternately, if the focus is on configuration design tradeoffs or optimization, the configurations parameters might be definitions of the wing shape. Finally, there are a host of CFD-analysis related parameters that have nothing to do with flight conditions or vehicle configuration. These may include grid refinement levels utilized in a grid resolution study, analysis fidelity (Euler, RANS, LES, etc.), turbulence models, CFD code used, date of analysis, etc. All of these parameters are inputs into the CFD analysis and, therefore, independent variables in the aerodynamic database and each adds a dimension to the parameter space. As a result, the number of dimensions in the parameter space can be very large.

Non-aircraft applications have a similar set of parameters. The flow conditions for a wind turbine may have wind speed, angle, and velocity profile (it is embedded in atmospheric boundary layer) while the configuration parameters may include blade pitch angle and rotation rate. Scalar output dependent variables would include forces and moments on the blades, which would be used in further analysis of the wind-turbine performance. Wind turbines, and other rotating machinery, have inherently unsteady periodic flow-fields that complicate the field-data analysis.

In a previous paper[1], the authors discussed the application of the generalized box-plot to dimensional reduction in the analysis of CFD meta-data. In this paper, we present an extension of the generalized function box plot for the visualization of four-dimensional unsteady data (x, y, z, t) , in a static three-dimensional data (x, y, z) image (or static images based on subsets of this data). This greatly simplifies the analysis of parametric studies of unsteady flow-fields.

The visual analysis of high-dimensional spaces is an active area of research. Ultimately, the data must be mapped to a two- or three-dimensional display in a way that is meaningful to the user. Standard CFD post-processing deals with three-dimensional data (x, y, z) , which is intuitive to the human visual cognition system, or four-dimensional data (x, y, z, t) , which is intuitive when animated. While animations are intuitive and effective in comparing local variations, it is difficult to visually synthesize global statistics from a long animation. In contrast, there is nothing intuitive about five-dimensional, or higher, spaces. The challenge of highly-dimensional data visualization is providing an intuitive understanding of both the local details and global extents of the data in one image. Existing strategies range from arrays of simple histograms, which don't display the dependency of the data on the independent variables, to complicated projection schemes and clustering algorithms. An example is the parallel-coordinate plot, which shows some of the relationships between variables, but is not typically used in the engineering world. Our strategy takes the functional box plot, a statistical technique used to visualize ensembles of one-dimensional functional results, and generalizes it to the projection of N-dimensional data statistics to one-, two-, or three-dimensional subspaces. In this paper, we focus on the application of the box plot to holistically summarize the unsteady properties of a flow field in a steady-state plot.

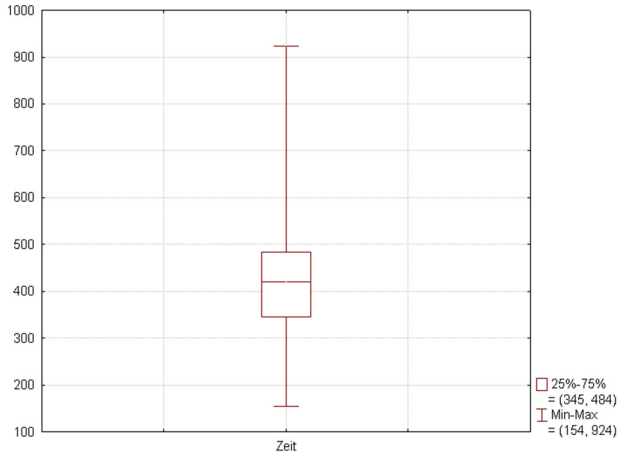


Figure 1. Basic box plot symbol (from Wikipedia).

The basic box plot symbol is shown in Figure 1. First developed by Tukey[2], it shows five descriptive statistics for a set of data values. The central line in the box is the median value, the lower and upper extent of the box is the 25th and 75th percentile values, and the ends of the lines above and below the box (also known as the whisker) are one set of several possible measures of the extent of the data. In some cases, these are the minimum and maximum values. In others, these are the 5th and 95th percentile. Throughout this paper, we will utilize the minimum and maximum values in our generalized box plots.

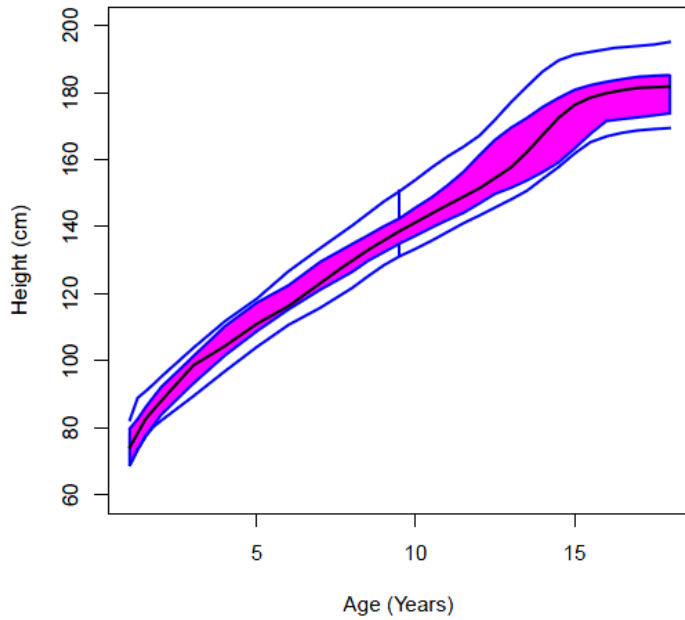


Figure 2. Functional Box Plot example.

A one-dimensional functional box plot is shown in Figure 2 (from reference 3). The functional box plot is an extension of the box plot concept to ensembles of one-dimensional functions. In this example, it was applied to measurements of height versus age of boys in France. The box plot is ultimately based on sorted data and the main difference between variants of the functional box plot is in how the data is sorted. In the simple case, the function is discretized, the results of the functions at the same value of the independent variable are sorted, and the values for the five statistics are used to

create the next segment of the lines for the five statistics. In other cases, the entire functions are sorted first.

For N-dimensional data visualization, the generalized functional box plot shows the variation of the same five statistics (minimum, first quartile, median, third quartile, and maximum) within conventional one-, two-, or three-dimensional plots. When combined with the same data for specific subspaces (sets of one, two, or three independent variables), the generalized box plot displays both the local variation of and a holistic view of the N-dimensional data.

2 Problem Statement

The generalized box plot is constructed using the following steps:

1. Of the N independent variables, X , define a subset, X_A , that are the active independent variables which the user wishes to retain. In unsteady flow, this is generally the spatial variables x , y , and z , plus any other parameter if it is a set of unsteady solutions from a parametric analysis.
2. Define the inactive subset of independent variables, X_I , as those you wish to summarize using the box-plot statistics. For unsteady flows, this is generally time.
3. For each point of X_A , sort by the dependent variable Y over all points in X_I and define the minimum, first quartile, median, third quartile, and maximum values.
4. On the plot in X_A , display the line, surface, or isosurface of the five statistics along with local Y data at a specific value of X_I .

This complexity of the algorithm is $O(n \log(n/k))$, where n is the total number of points in parameter space and k is the number of points in the active subspace.

Frequently the parametric data is not full factorial and must be resampled to an N-dimensional rectangular array before this algorithm is applied. The resampling is generally based on a kriging or response surface surrogate model for the variation of Y with X . This works well unless the parametric space is inherently non-rectangular. In this case, a more complex form of resampling is required.

2.1 Results for Meta-Data Dimensional Reduction

As a first example, we will demonstrate the box-plot for reducing the dimensionality of meta-data in an high-dimensional parametric space. The application of the box-plot for unsteady data is in section 2.2.

The generalized functional box plot has been tested on the meta-data from two collections of CFD meta-data: force and moment data from a parametric study of the BEES Flyer[1,4,5] and the force and moment data from the 2010 High Lift Prediction Workshop[1,6,7].

2.1.1 BEES Flyer Parametric Study

The first example is an aerodynamic database for the bio-inspired engineering of exploration systems (BEES) flyer[5]. This system was envisioned as a small autonomous flying vehicle, with an adaptive control system mimicking those of biological systems, for the exploration of Mars. The geometry, show in figure 3, has a triangular planform with a set of vertical fins at the wing tips. It has a set of two elevons for pitch and roll control.



Figure 3. Prototype of BEES flyer geometry (cf. Ref. 4 for details)

Murman, et. al.⁴ created a 5-dimensional aerodynamic database for this configuration using the CART3D Euler code. They used a full-factorial (5D rectangle) experimental design with the following parameters:

Configuration Space:

Parameter	Values	Number of values
Left elevon deflection (δL)	-10 deg to 20 deg. in 5 deg. increments	7
Right elevon deflection (δR)	-10 deg to 20 deg. in 5 deg. increments	7

Flight Parameter Space:

Parameter	Values	Number of values
Mach Number (M)	0.2, 0.3, 0.4, 0.5, 0.6, 0.7, 0.75, 0.8	8
Angle of Attack (α)	-10 to 15 in 5 deg. increments	6
Yaw Angle (β)	0 deg. And -10 deg.	2

In total they solved the Euler equation for 4,704 discrete conditions. They visualized the field data results for M, α , and β held constant using an array of 49 (7x7) contour plots, and visualized surfaces of CL and CM versus both elevon deflections for M=0.6, $\alpha=5.0^\circ$, and $\beta = 0.0^\circ$. This visualization, with the addition of the coefficient of rolling moment, is duplicated in Figure 5.

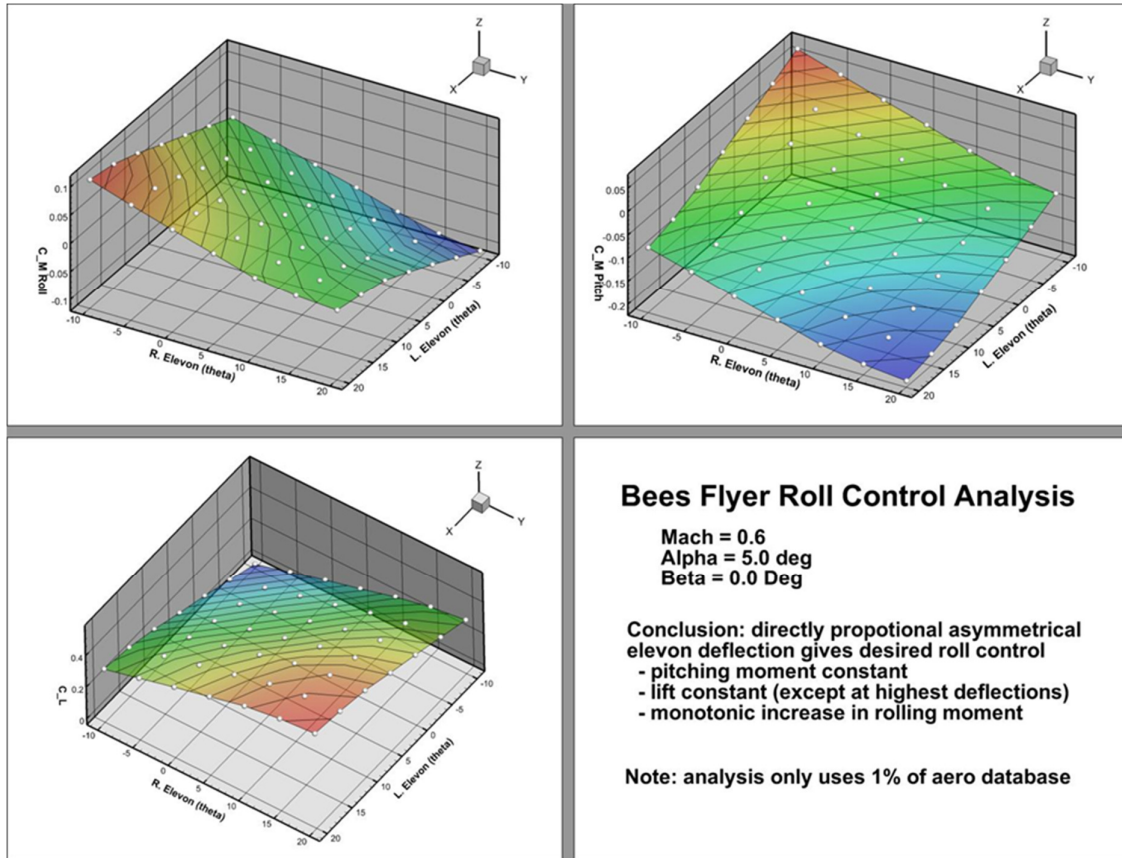


Figure 4. BEES Flyer Roll Control Analysis.

The purpose of Figure 4 is to analyze the roll control of the BEES flyer during deflection of the elevons. Note that a directly proportional, asymmetrical, deflections ($\delta L = -\delta R$) of the elevons result in the desired rolling moment with little change in the lift or pitching moment. This is the desired behavior – no pitching generated or required during a rolling maneuver. Note however, that this conclusion is based on only 1% of the aerodynamic database. Does it behave similarly at other values of M , α , and β ?

Figure 5 shows a surface generalized box plot for rolling-moment coefficient. It displays five surfaces for minimum (purple), first quartile (blue), median (color flooded contours), third quartile (yellow), and maximum (pink) based on all of the data over the inactive variables (M , α , and β) for each combination of δL and δR . It also displays the original surface shown in Figure 5. There is a significant spread over the inactive variables, but the trends seem to hold over the entire dataset. To be sure it would be necessary to investigate further, perhaps using filters which alter the range of M , α , and β to interactively explore the impact on the surface box plot.

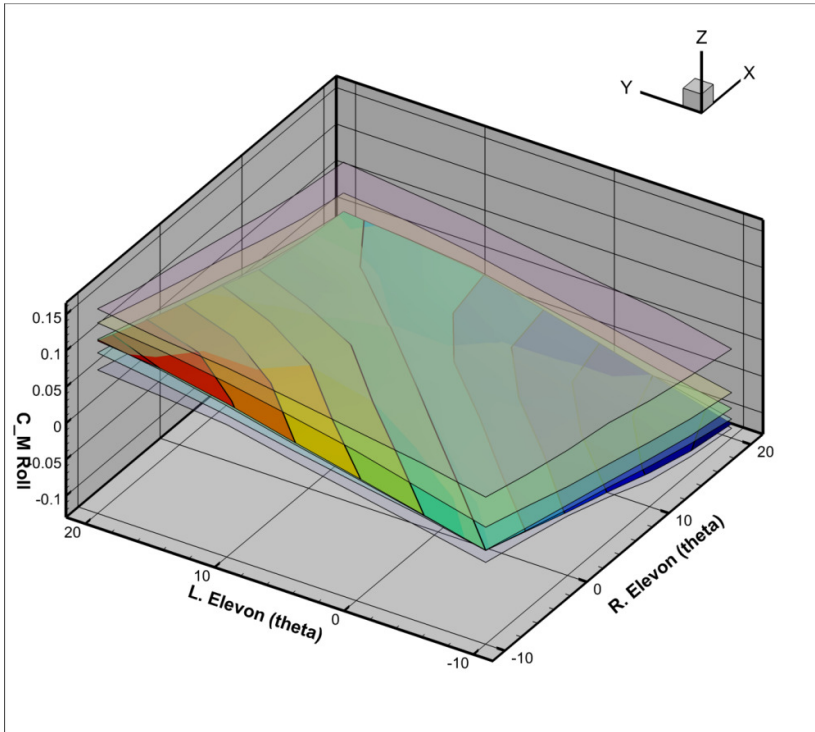


Figure 5. Generalized surface box plot for rolling moment coefficient of BEES flyer

Figure 6 shows a surface box plot for the lift coefficient. As you might expect, lift coefficient is strongly influenced by one of the inactive variables, α , and the result is a large spread in the box plot statistics. While the data appears to have the desired trends, it would not be wise to base any design decisions on this plot alone.

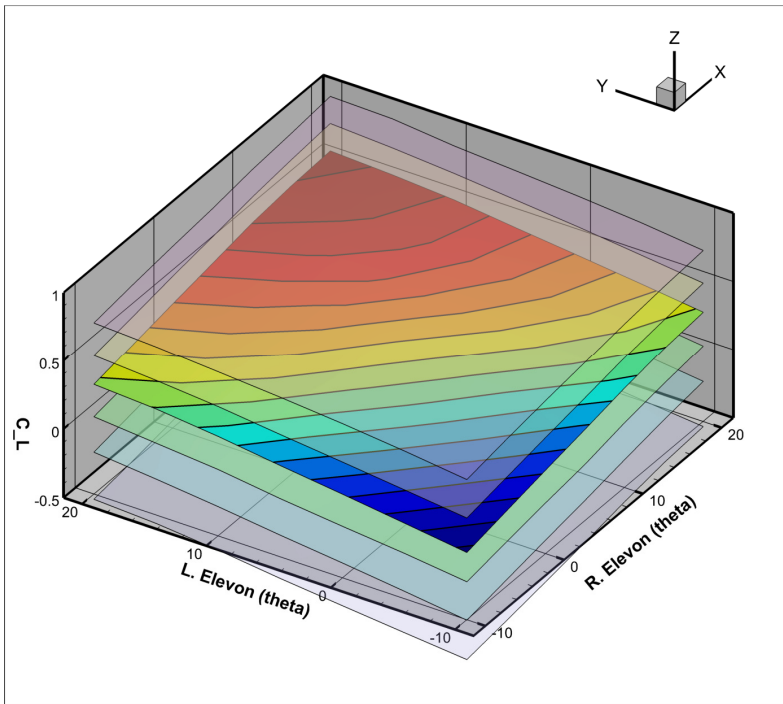


Figure 6. Generalized surface box plot for lift coefficient of BEES flyer

2.1.2 High Lift Prediction Workshop Forces and Moments

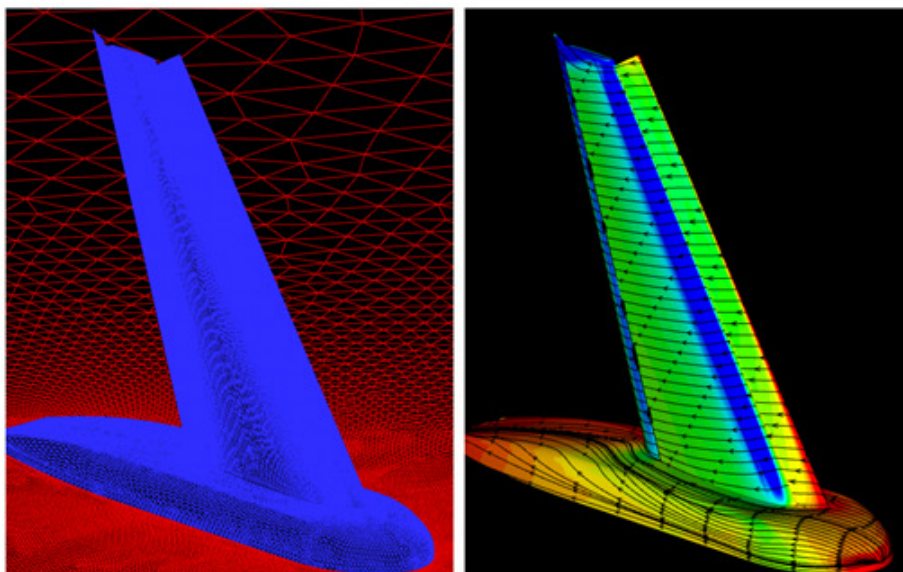


Figure 7. Grid and computed flow properties for the NASA Trapezoidal Wing configuration used in the High Lift Prediction Workshop (image from <http://hiliftpw.larc.nasa.gov/Workshop1/geometries.html>).

The second example is force and moment data from the first High Lift Prediction Workshop[6,7]. The 2010 workshop contained three cases: a mandatory grid convergence study, and mandatory flap deflection prediction study, and an optional flap and slat support effects study. The geometry used was the NASA Trapezoidal Wing configuration, for which substantial wind-tunnel data has been collected. The workshop was held at the AIAA Applied Aerodynamics Conference in August 2010. The result was 35 datasets, submitted by participants in 18 individual organizations.

The force and moment data from these 35 datasets represents a far less structured collection of data than from the BEES-flyer database. The grid resolution study required runs with 3 or 4 grid resolutions at two angles-of-attack and fixed M , Re , flap angle, and slat angle. The flap deflection prediction study contained a sweep over seven angles-of-attack and two flap angles, with everything else held constant. Finally, the optional support effects study involved two support configurations (there or missing) with everything else held constant. In addition, of course, the participants used a variety of CFD codes, with differing solution schemes, solving variations of the Navier-Stokes equations, with a variety of turbulence models. Each of these four items could also be considered an independent variable in the overall database. The result is a database with up to seven independent variables: angle-of-attack, grid resolution, flap angle, CFD code, solution scheme, Navier-Stokes variant (thin layer, etc.), and turbulence model.

The comparisons of the results with experiment were primarily done with arrays of XY plots. Because the generalized box plot could show the statistics for the entire database on one plot per dependent variable, it can dramatically reduce the number of plots required to quantitatively compare datasets. The surface box plots for C_L versus α and flap angle is shown in figure 9. The central surface with flooded contours is the median values, the light blue surface are the first and third quartiles, and the outer translucent surface are the minimum and maximum. The central 50% of the datasets are closely packed for angles-of-attack below stall. Above stall there is significant divergence. The minimum surface diverges at a much lower angle-of-attack and warrants further investigation. The box plot doesn't show which dataset is responsible for the divergence of the minimum surface at the low angle-of-attack, or even how many datasets contribute to the surface.

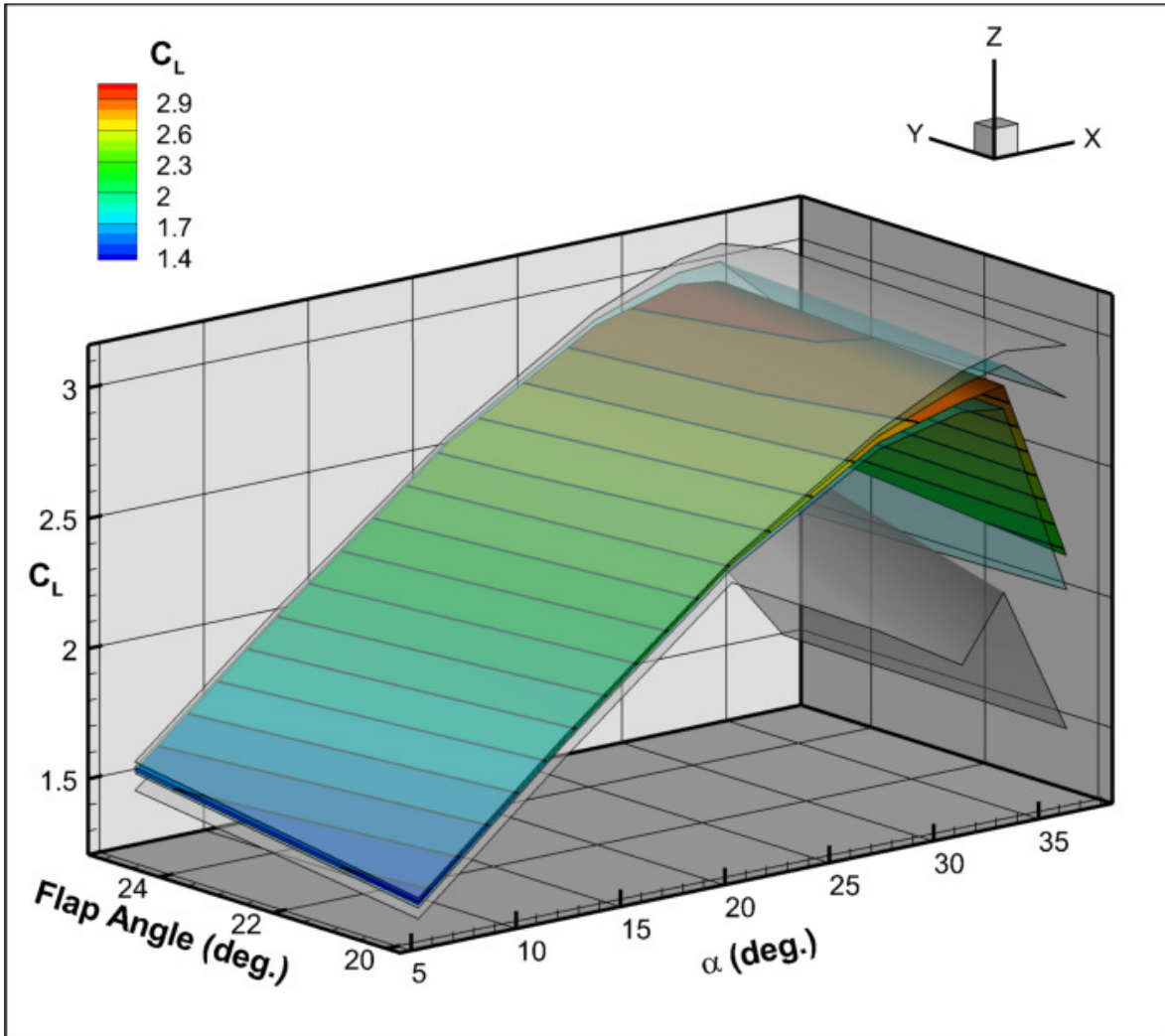


Figure 8. Surface box plot for lift coefficient versus angle-of-attack and flap angle.

The line functional box plots for configurations 8 and 1 (flap angles 20 and 25 deg.) are shown in figures 9 and 10. These correspond to the minimum and maximum flap-angle edges of the surface box plot in figure 8. Figures 9 and 10 also include experimental data for comparison. It is clear from these figures that the majority of CFD codes do a good job predicting lift at angle-of-attacks below stall, but there is significant divergence above stalling angle-of-attack.

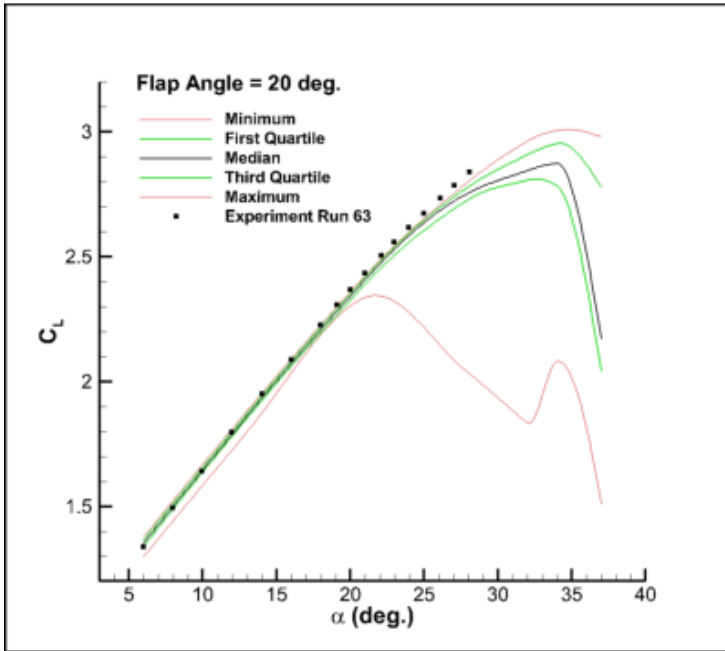


Figure 9. Line functional box plot for lift coefficient versus angle-of-attack at 20 degree flap angle.

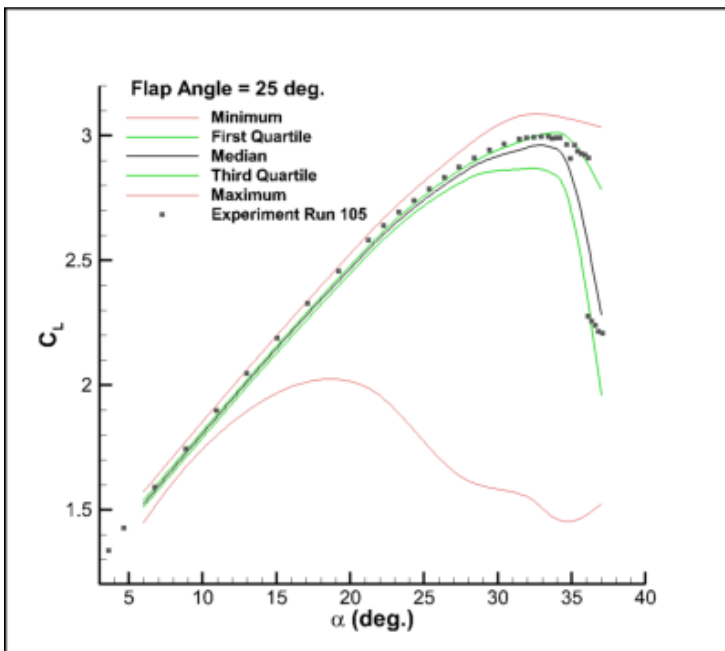


Figure 10. Line functional box plot for lift coefficient versus angle-of-attack at 25 degree flap angle.

The results are very similar for drag (figures 10, 11, and 12), with the majority of datasets closely matching the experimental data for angles-of-attack below stall. For pitching moment (figures 13, 14, and 15) it is a different matter. The box plots show the CFD codes systematically predict higher (less negative) values of pitching moment. The analysis indicates that you should not trust pitching-moment predictions from the codes and grids used in the high lift prediction workshop.

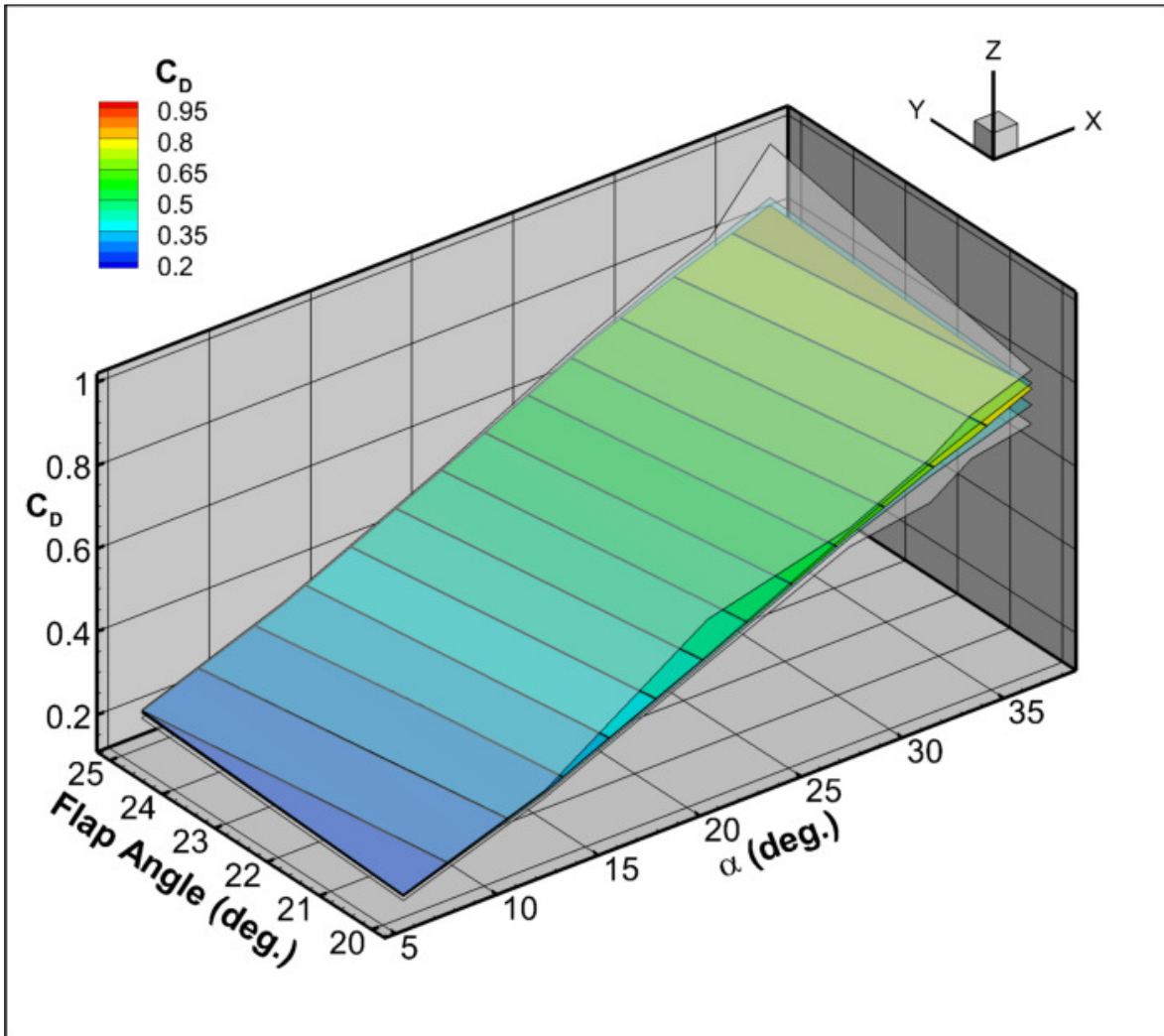


Figure 10. Surface box plot for drag coefficient versus angle-of-attack and flap angle.

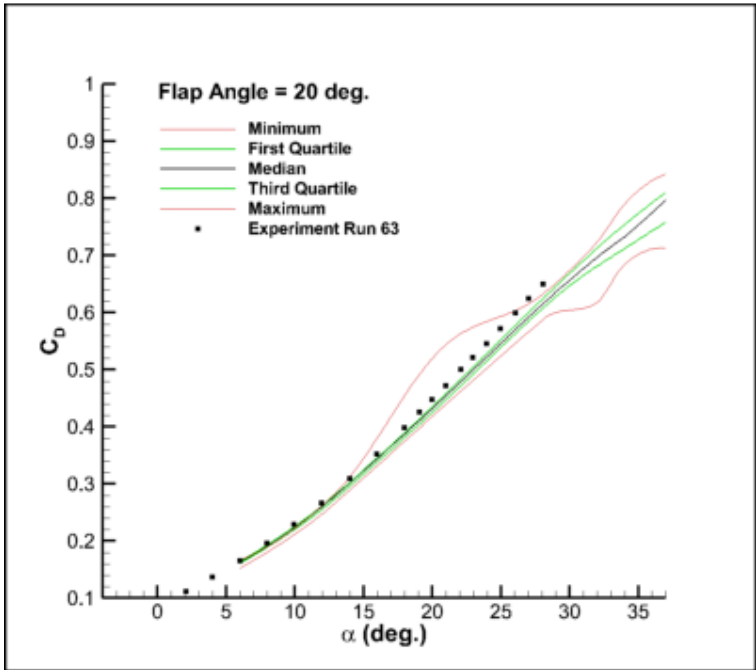


Figure 11. Line functional box plot for drag coefficient versus angle-of-attack at 20 degree flap angle.

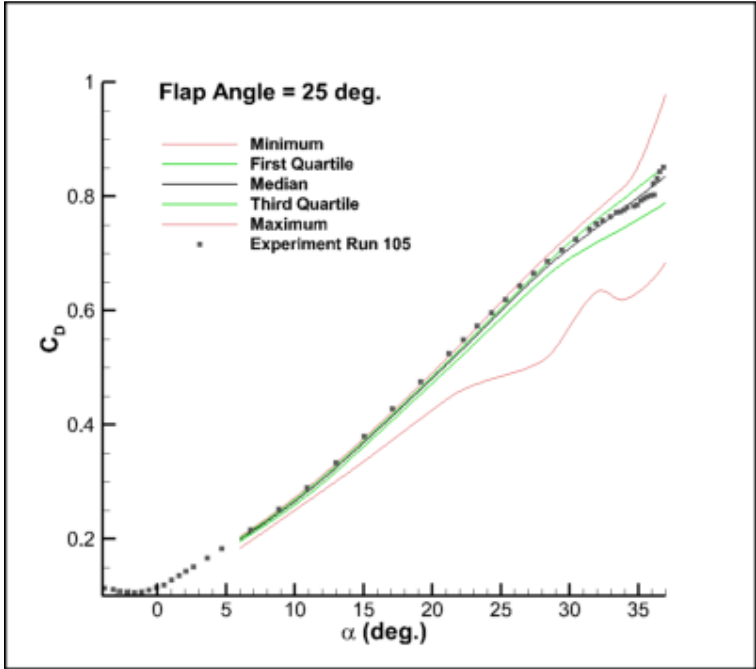


Figure 12. Line functional box plot for drag coefficient versus angle-of-attack at 25 degree flap angle.

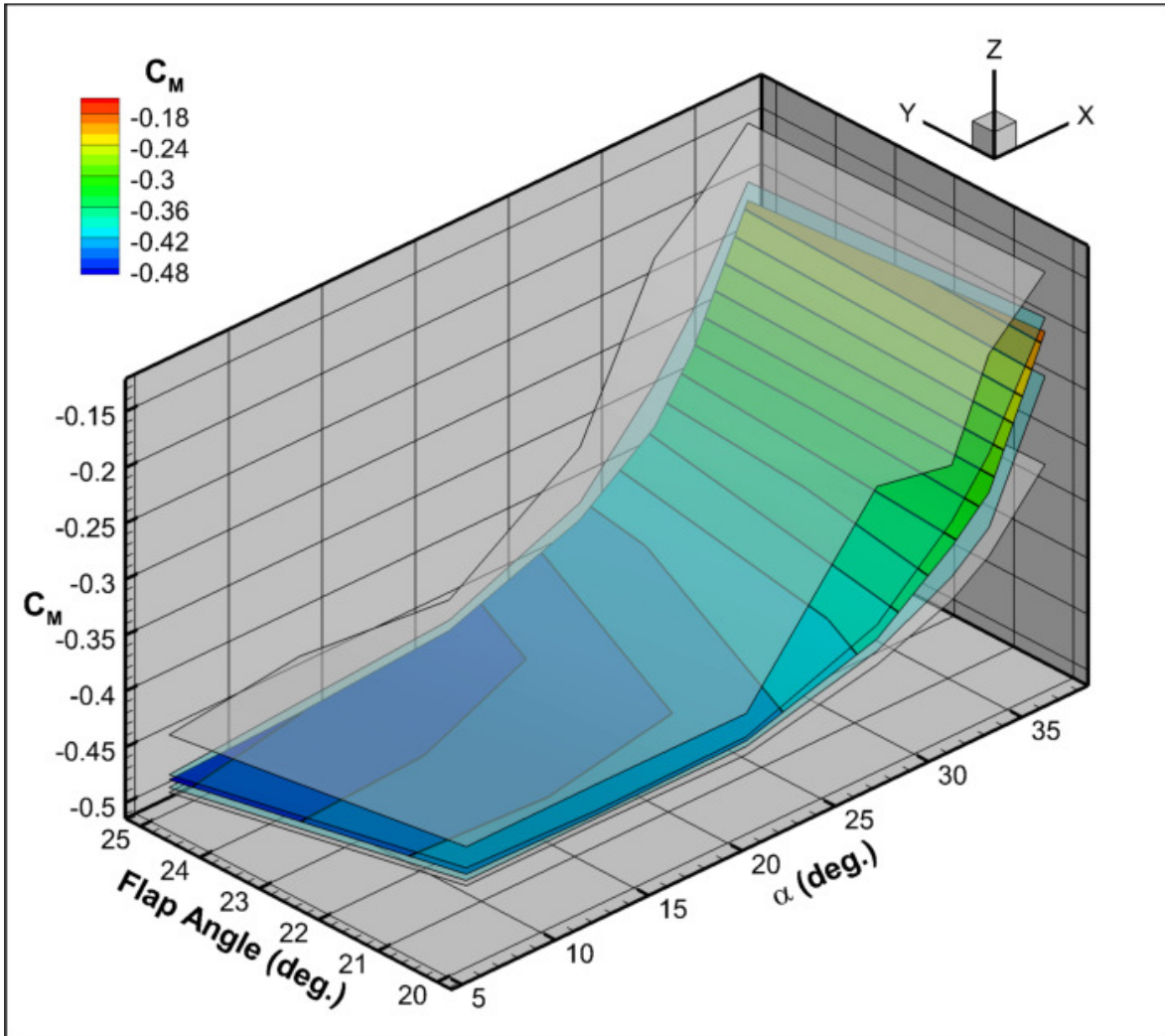


Figure 13. Surface functional box plot for pitching-moment coefficient versus angle-of-attack and flap angle.

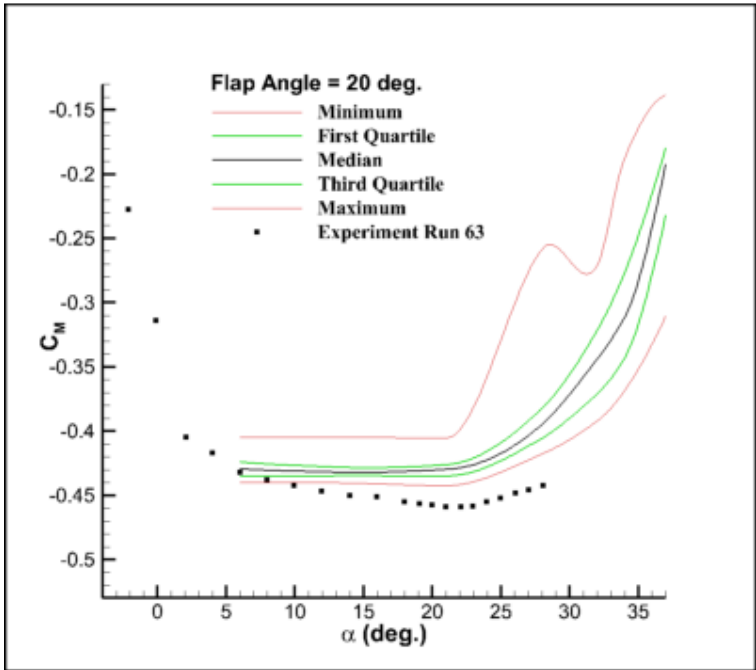


Figure 14. Line functional box plot for pitching-moment coefficient versus angle-of-attack at 20 degree flap angle.

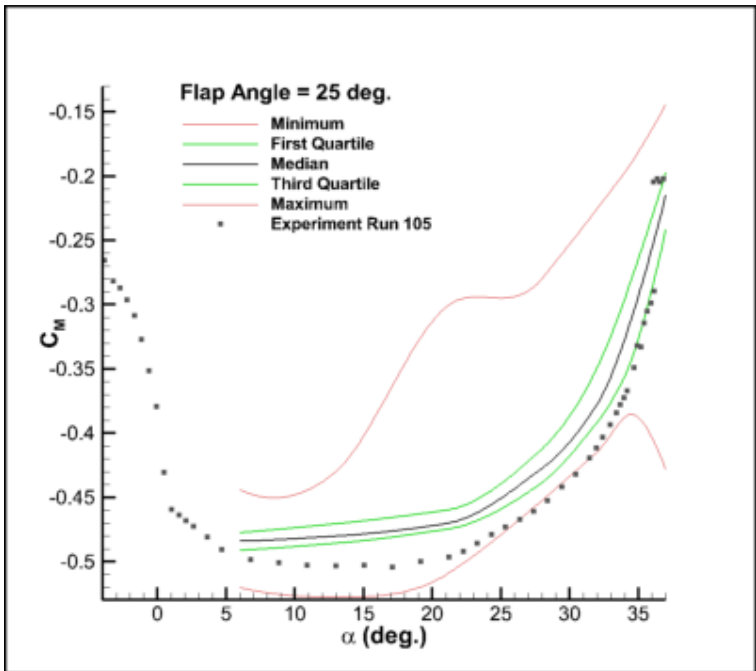


Figure 15. Line functional box plot for pitching-moment coefficient versus angle-of-attack at 25 degree flap angle.

2.2 Results for Unsteady CFD Flow Data

For four-dimensional unsteady data visualization, the generalized functional box plot shows the variation of the same five statistics (minimum, first quartile, median, third quartile, and maximum) over time for each point in the field. The statistics can be displayed in conventional one-, two-, or three-dimensional plots. The results may be combined into a single plot with 5 surfaces, or 5 plots showing the variation of the five statistics over the field.

The box plot is a powerful tool for analyzing unsteady flow. In a single plot it shows the range over time of each variable, at each point in space. This information has many direct applications. Frequently, the engineer is concerned about certain variables exceeded some limit value. For example, a box plot of temperature on the surface of a turbine blade will quickly tell the engineer if it has exceeded the melting temperature of the material and any time in the analysis. Likewise, the degree of oscillation (min to max) may be significant in certain chemical processes. Finally, the box plot allows rapid side-by-side evaluation of several unsteady cases that would otherwise be very difficult to compare.

2.2.1 Vortex Shedding from Swept Cylinder (LES)

The first example is unsteady flow past a swept cylinder. The 0.25m diameter cylinder is swept upward (positive y direction) by 50 degrees and backward (negative x direction) by 30 degrees. The cylinder is situated between two free-slip walls 1.22m apart. The free-stream flow conditions are Mach 0.1 and Reynolds number of 58784.7. The computation assumed laminar flow.

Figure 16 shows the generalized functional box-plot for X-component of momentum on a slice aligned with a swept cylinder. The flow is going from right to left (positive X direction). Upstream of the cylinder, all of the statistics align (no unsteadiness). The statistics separate significantly just downstream of the cylinder where the unsteadiness is at a maximum, and slowly converge as the distance downstream of the cylinder increases.

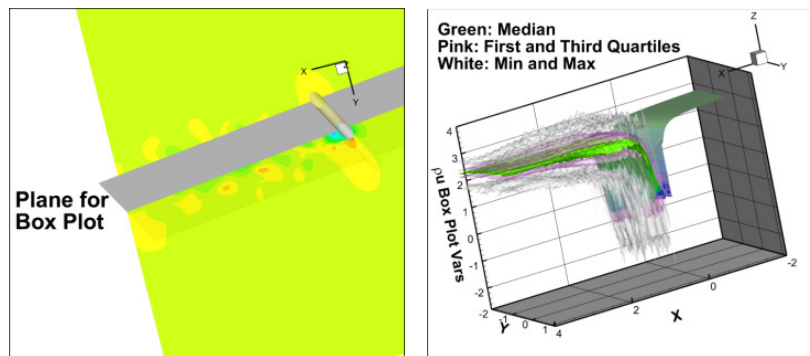


Figure 16. (left) Unsteady flow past a cylinder, (right) x-momentum box plot on plane

From this box plot, it is easy to see the extent of the oscillations in the x-momentum at each point in the field.

2.2.2 Wind-Turbine Acoustics

Modern industrial economies are heavily reliant on electricity, and developing and maintaining a sufficient supply of affordable and reliable power generation capability is a priority of every nation. Fossil fuel based power generation capabilities have become less attractive for environmental reasons and the future expansion of nuclear power is uncertain following the recent Fukushima nuclear accident. For all of these reasons, “environmentally friendly” wind and solar power have become more attractive.

One of the largest issues with wind-turbines is noise. For this reason, Nelson, et. al., recently

published a study that used a sequence of numerical methods to predict the noise pattern from wind-turbines[8]. The sequence starts with a solution of the Navier-Stokes equations for the unsteady flow-field around the NREL 10m diameter research wind turbine (figure 17). The equations were solved using the OVERFLOW code with adaptive mesh refinement. The computational grid started with a 30.5 million point mesh (in 68 blocks) and over 7152 time steps grew to over 260 million points in more than 5600 blocks. The results were exported to plot files every 16 time steps for further analysis. In all, the plot files consumed roughly half a terabyte of disk space.

The case modeled had a blade pitch of 3 degrees, a constant inflow velocity of 10 m/s and the wind turbine was perfectly aligned with the freestream. A complete evaluation of noise production over the complete operating envelope of the wind turbine would require a parametric analysis with multiple dimensions for blade pitch, wind speed, wind profile, and wind alignment with the turbine. While a single case may be analyzed with conventional techniques like animation of slices and isosurfaces, the complete parametric study would require aggregation of cases to reduce the number of dimensions. This is the purpose of the generalized functional box plot.



Figure 17. The NREL 10M research wind turbine

Figure 18 shows the components of the generalized functional box plot for vorticity magnitude on a plane at $x=2.5\text{m}$ downstream of the blade. The box plot was generated by interpolating to a rectangular 500×500 plane at each available time step for the last half rotation of the blade. The vorticity magnitude at each point was sorted through time, and the minimum, first quartile, median, third quartile, and maximum values at that point were extracted. This maximum plot shows an intense tip vortex, and intense vortex sheet shedding from the pylon, and a complicated pattern of vortices shedding from the blade. For vorticity magnitude, the minimum, first quartile, and median plots show little detail of additional value.

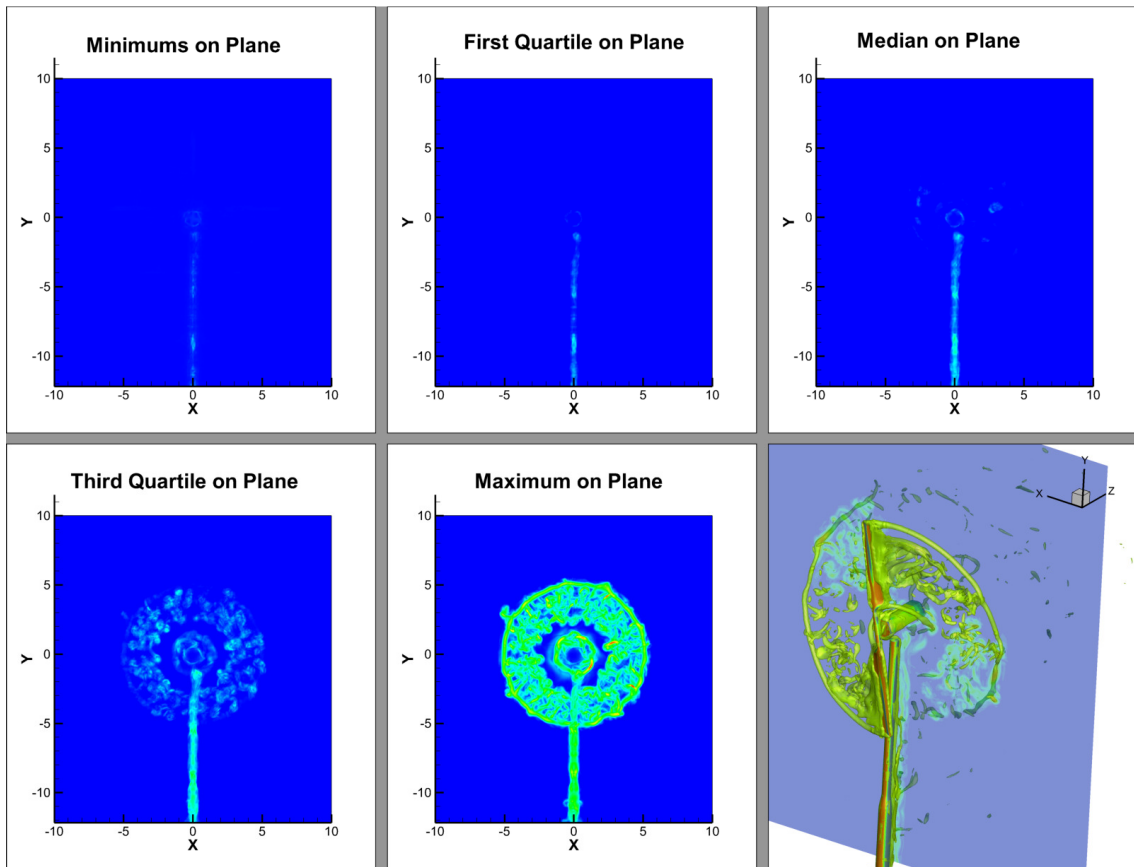


Figure 18. Vorticity box plot components.

Figure 19 shows the components of the generalized functional box plot for pressure on the plane $x=2.5\text{m}$ downstream of the blade. They show that, on this plane, the most intense pressure oscillations are occurring near the base of the pylon. The cause of this is unknown. It could be a physical phenomenon, such as a feedback loop with fluctuations emanating from the rotors bouncing off the ground and interacting with the mast, or it could be a numerical artifact. The most important fact, from the standpoint of this paper, is that these results were intensively analyzed using traditional visual analysis techniques, and this phenomenon was not discovered until the functional box plot was created.

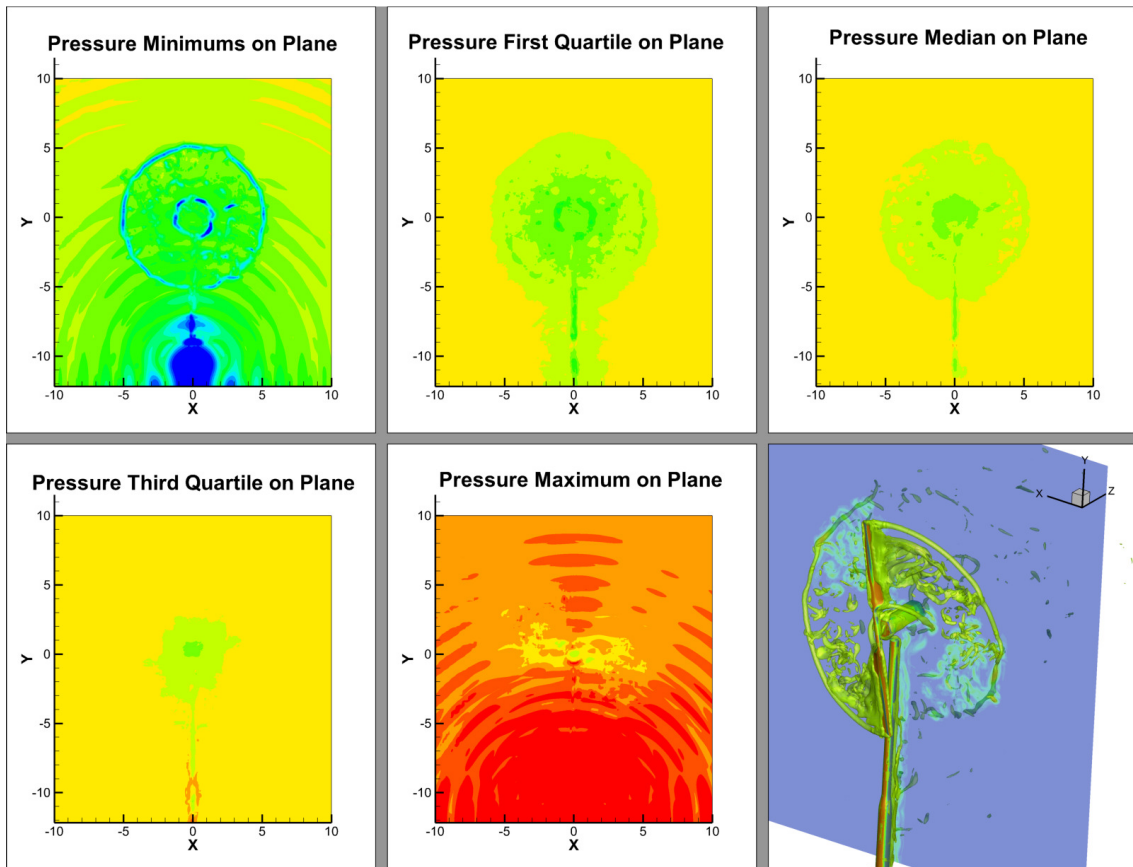


Figure 19. Pressure box plot components.

3 Conclusion and Future Work

The function box plot was generalized to analyze and visualize the statistics of N-dimensional meta-data and unsteady flow fields. The technique for meta-data was demonstrated for a roll-control analysis of the five-dimensional BEES-flyer aerodynamic database and for comparative analysis of the first High Lift Prediction Workshop database. For unsteady flows, the technique was demonstrated for vortex shedding off a swept cylinder and for flow past a wind turbine. The generalized function box plot is a powerful tool for generating a holistic view of highly dimensional meta-data and unsteady flows.

References

- [1] S. T. Imlay and C. A. Mackey. Generalized Functional Box Plot for Visual Analysis of High-Dimensional Aerodynamic Meta-Data. AIAA 2012-1262, Jan. 2012.
- [2] J. W. Tukey. Box-and-whisker plots. *Exploratory Data Analysis*. Addison-Wesley, Reading MA. 1997. pp 39-43.
- [3] Y. Sun and M. G. Genton. Functional Boxplots. *J. Computational and Graphical Statistics*, 20:216-334, 2011.
- [4] S. M. Murman, M. J. Aftosmis and M. Nemec. Automated Parameter Studies Using a Cartesian Method. AIAA 2004-5076.
- [5] D. D. Soccol, J. S. Chahl, J. Le Bouffant, M. A. Garratt, A. Mizutami, S. A. Thurrowgood, G. Ewyk, and S. Thakoor. A Utilitarian UAV Design for NASA Bioinspired Flight Control Research. AIAA Paper 2003-461, Jan. 2003.

- [6] J. P. Slotnick, J. A. Hannon and M. Chaffin. Overview of the First AIAA High Lift Prediction Workshop. AIAA 2011-0862, Jan. 2011.
- [7] C. L. Rumsey, M. Long, R. A. Stuever and T. R. Wayman. Summary of the First AIAA CFD High Lift Prediction Workshop. AIAA 2011-0939, Jan. 2011.
- [8] C. C. Nelson, A. B. Cain, G. Raman, T. C. Chan, R. M. Saunders, J. Noble, R. Engeln, R. Dougherty, K. S. Brentner, and P. J. Morris. Numerical Studies of Wind Turbine Acoustics. AIAA 2012-0006, Jan. 2012.